JOURNAL OF SPACECRAFT AND ROCKETS
Vol. 36, No. 5, September–October 1999

Performance Study of a Power Law Starbody

John W. Sabean* and Mark J. Lewis†
University of Maryland, College Park, Maryland 20742-3015
and
David Mee‡ and Allan Paull§
University of Queensland, Brisbane, Queensland 4072, Australia

The performance of a power law starbody, designed for low drag, was calculated numerically and verified experimentally. The methodology of the design shape is presented along with a comparison to other forebody shapes and an evaluation of scaling effects. A starbody was constructed and tested in the University of Queensland reflected shock tunnel, T4. Various test conditions were used to determine both the on-design and off-design performance of the starbody. These results are compared with those of tests done on a cone of equivalent volume and length. The resulting starbody shape is shown to have 20% less drag than the equivalent cone at a Mach number of 6.4 and an $Re = 1.5 \times 10^6$.

Nomenclature

C = scaling factor for power law curve, where y is $Cx^{3/4}$
L = length of body, m
n = number of fins
P_∞ = freestream pressure, Pa
R_{eff} = radius of an equivalent volume cone, m
T_∞ = freestream temperature, K
ρ_∞ = freestream density, kg/m^3

Introduction

PREVIOUS studies have shown that nonaxisymmetric bodies may offer reduced wave drag as compared to simple bodies of revolution.[1] A promising category of these nonaxisymmetric shapes is the so-called starbodies. Both theoretical and experimental efforts have been performed on starbodies with planar side panels, also referred to as wedge-derived starbodies, such as those presented by Vedernikov et al.[2] and Zubin et al.[3] Such shapes, at on-design conditions, produce a two-dimensional flowfield between the fins, with an attached shock at the edge of each fin. It has been shown that these starbodies have lower wave drag than an equivalent circular cone with the same length and volume. The tradeoff for these shapes is the larger viscous drag due to the increased surface area associated with the fins. As such, starbody shapes tend to have larger viscous drag than cones of equivalent volume and length.

Most studies of starbodies have focused on wedge-derived forms because they can be derived analytically, but there is no reason to believe that these forms represent minimum drag forms. In fact, there are many options available for producing starbody shapes, some of which may have even lower drag than the wedge-derived forms. Several efforts have attempted to examine general starbodies using Newtonian flow, and they suggest that the optimum star shape would be one with a longitudinal contour that is a $\frac{3}{4}$-power law.[1] This study goes further to determine that the fin shape should be a concave shape, such as that shown in Fig. 1. Another more recent numerical study, also using Newtonian flow, by Foster and Dulikravich[4] seems to confirm this result.

Received 14 April 1998; revision received 15 November 1998; accepted for publication 2 December 1998.

*Graduate Research Assistant, Department of Aerospace Engineering. Student Member AIAA.
†Associate Professor, Department of Aerospace Engineering. Associate Fellow AIAA.
‡Senior Lecturer, Centre of Hypersonics, Department of Mechanical Engineering.
§Senior Research Fellow, Centre of Hypersonics, Department of Mechanical Engineering.

As pointed out by Chernyi and Gonor,[1] limitations of the Newtonian solution cause the pressure at the centerline, between the fins, to be underpredicted, introducing inaccuracy into the solution. Experimental results with wedge-derived starbodies suggest other problems with the Newtonian solution as well; for a wedge-derived starbody, at Mach numbers significantly higher than design, a lambdalike shock structure is formed as the attached shock moves down between the fins, as shown in Fig. 2 (Ref. 3). Such a structure would be even more likely to form given the concave fin shape shown in Fig. 1. This shape was produced by a Newtonian solution, which cannot predict this type of shock structure. Thus, these Newtonian-derived shapes would most likely perform well for lower Mach numbers but have drag much higher than predicted at higher Mach numbers.

The lambda shock structure can be avoided by ensuring that the shock is attached to the fins. This can be done by taking the $\frac{3}{4}$-power law profile of the desired centerline as a flowfield generator and using inverse design methods to create a three-dimensional shape with an attached shock.[5] In the present work, a finite volume computational fluid dynamics (CFD) code is used to calculate the flow over a two-dimensional $\frac{3}{4}$-power law shape. This solution is then used to generate the star fin shape. Between each fin, the resulting starbody will have the same two-dimensional flow as in the original CFD solution, as well as an attached shock wave. Because the derived flowfield is constructed from a known initial flow, the on-design performance of these bodies can be readily determined.

A starbody was designed and tested in the T4 reflected shock tunnel at the University of Queensland. The predicted drag performance is compared to the experimental results. Several tests were done at various conditions to test the off-design performance of these types of shapes.

Design Methodology

Numerical Formulation

The General Aerodynamic Simulation Program (GASP)[6] is used to generate the flowfield in the inverse design process. This finite volume code is used to solve the two-dimensional Euler equations over a power law shape with the form $y = Cx^{3/4}$ for various values of C. The grid is generated algebraically using the same functional form, with clustering near $x = 0$, to better capture the flow properties at the nose. The grid is also broken into two zones: a subsonic zone with 45×51 grid points and a supersonic zone with 56×70 grid points. A sample grid is shown in Fig. 3. The calculations in the supersonic zone are done using space marching to lower the overall runtime required per calculation. As such, a complete calculation requires only 15–20 CPU minutes on a DEC Alpha 600/266. The results from a sample calculation are shown in Fig. 4.

The flow is calculated in the subsonic region using Van Leer flux vector splitting with a min–mod limiter and is globally iterated

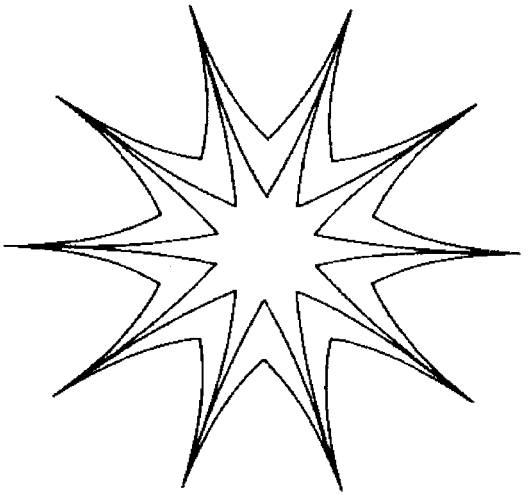

Fig. 1 Examples of starlike solutions (from Ref. 1).

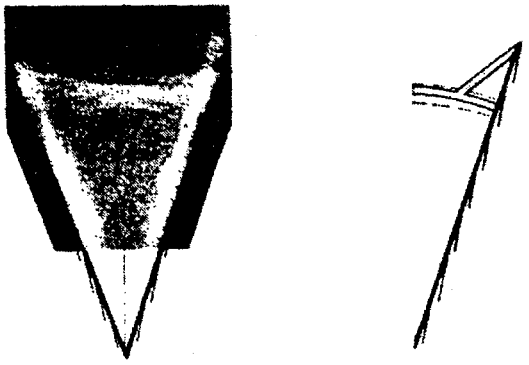

Fig. 2 Lamda shock structures on wedge star bodies (from Ref. 3).

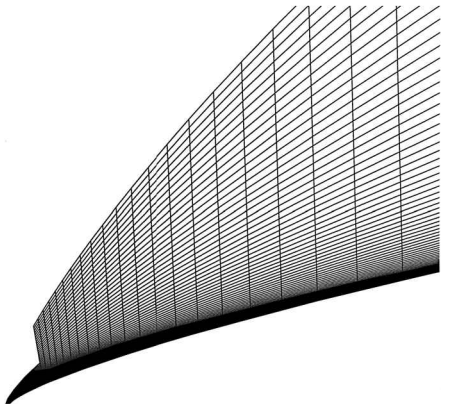

Fig. 3 Sample grid for two-dimensional power law body calculation.

using a two-factor approximate factorization (AF) method. The supersonic region uses a full flux in the marching direction, with a catastrophic limiter based on the pressure and density of the flow in the transverse direction, as well as a first-order-accurate lower–upper decomposition on a single line with relaxation in the sweep direction. Inviscid wall boundary conditions are used because the final body surfaces are in locations very different from those of the generating surface. The flow is assumed to be nonreacting air with a constant value of $\gamma = 1.4$.

Inverse Design

The application of inverse design methods to the creation of starbodies is similar to the technique used to determine so-called waveriders.[7] In fact, a starbody is several waveriders joined at the

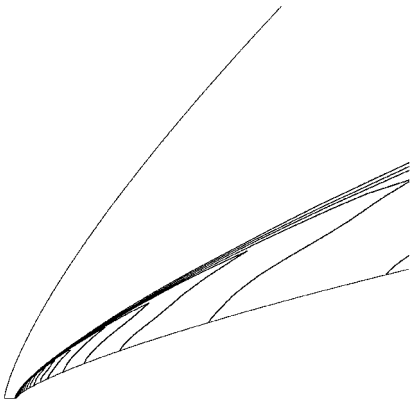

Fig. 4 Pressure contours at Mach 6.4 for two-dimensional power law body sample calculation.

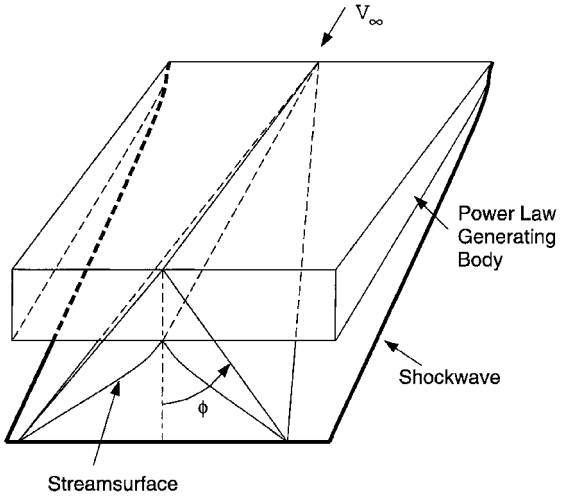

Fig. 5 Construction of a power law waverider section, after Rasmussen.[8]

leading edges. The design method involves using a known flowfield with a shock wave and choosing the shape of the body to correspond with the stream surface that intersects the shock wave and a chosen planform. In the case of typical waveriders, this generating flowfield is that associated with either a two-dimensional wedge or an axisymmetric cone, from which a nearly infinite number of planforms can be selected, each corresponding to a different waverider shape. Optimization techniques can be used to find the waverider with the maximum value of some figure of merit, such as lift-to-drag ratio or volumetric efficiency.

For the design of a power law starbody, the flowfield generator is the two-dimensional $\frac{3}{4}$-power law body described earlier. The flowfield is determined numerically with the described code, and the planform is chosen such that n identical shapes can be placed end to end in a star shape, where n is the number of fins desired. The method for generating the body shape is similar to the method for constructing a caret waverider, as detailed by Rasmussen.[8] The relation of the generating flowfield with the generated body is shown in Fig. 5. The angle ϕ describes the planform and is determined by the number of fins n. In the case of $n = 4$, ϕ would equal 45 deg. With the planform chosen, the stream surface is then determined by tracing streamlines through the numerical solution, starting at the intersection of the desired planform with the shock. The shock wave position is determined by locating the position of the largest pressure gradient along a grid line normal to the body surface. The streamline is traced by stepping through the flowfield with step sizes based on the local grid cell size. The flow properties at each point are interpolated from the values at the surrounding grid points. An example of a resulting starbody is shown in Fig. 6. Note that typical waverider-generating flowfields are hyperbolic and do not contain subsonic regions. The concept of inverse design is dependent on the

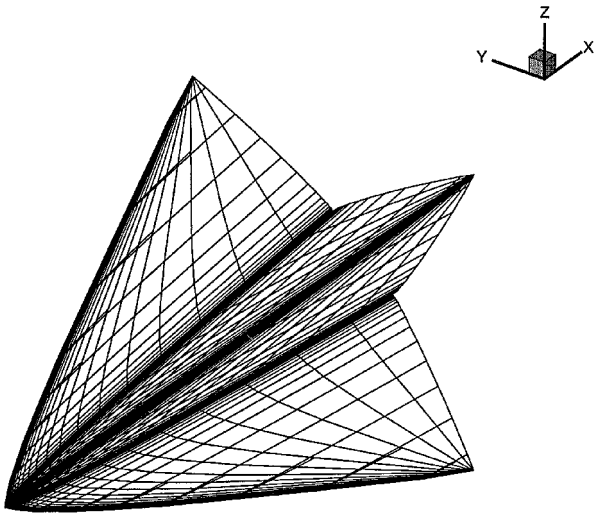

Fig. 6 Mach 6.4 designed $\frac{3}{4}$-power law starbody.

hyperbolic nature of the flowfield. In the present work, streamlines near the nose of the star are traced through a subsonic region and used to produce the body surface. This approximation did not cause any significant changes in the flowfield due to the small size of the subsonic region relative to the length of the body. For more blunted power law shapes with larger subsonic regions, however, this approximation will break down.

The use of a known flowfield allows the on-design performance of these starbodies to be readily determined. The fluid properties at the wall of the design correspond to the fluid properties of the chosen stream surface. The pressure can then be integrated over the surface of the body to determine the wave drag acting on the body. For simplification, the pressure acting on the rear of the body is assumed to be zero. The temperature on the surface is also known and can be used with a reference temperature method [9] to determine an approximate value of the viscous drag. The drag on the body is assumed to be completely laminar, and the wall temperature is assumed to be equal to the ambient temperature T_∞. For purposes of comparison to other results, the volume, effective radius, and wetted surface area are calculated for each body.

Grid Dependence

To determine the sensitivity of the various figures of merit to the number of grid points chosen in the original CFD solution, a grid dependence analysis was performed. The number of grid points was doubled in both the i and j directions. Each of the figures of merit were calculated for the same conditions for various generating body sizes. The largest difference was in the wave drag, which was found to be overpredicted by 3–5%. The volume was found to be overpredicted by 2–3%. The other figures of merit varied by less than 1%. From these results, it was decided that the chosen number of grid points was sufficient for this study.

Numerical Validation

To verify the validity of the results further, it was decided to do a full three-dimensional CFD calculation. This calculation also uses GASP[6] to solve the three-dimensional Euler equations. This solution uses two grids, both a subsonic region and a supersonic region, so that space marching can be used to speed the calculations in the supersonic region. The subsonic region used $55 \times 28 \times 50$ grid points and was globally iterated using a three-factor AF method, whereas the supersonic region used $99 \times 73 \times 50$ grid points and used space marching with a two-factor AF method. The chosen limiters and fluxes remained the same as with the two-dimensional case to obtain a consistent result. The calculations were done on a Cray J-90 and required approximately 2 CPU hours of runtime to obtain a solution.

A sample result for the flow between two fins is shown in Fig. 7. Figure 7 shows pressure contours for planes perpendicular to the flow direction. As can be seen, there is a distinct two-dimensional shock wave attached to the edge of the fins. The contours are qualitatively identical to the two-dimensional solution. For a quantitative comparison, the pressure over the surface of the body is integrated to determine the wave drag predicted by the three-dimensional solution. The value of the wave drag predicted by the three-dimensional test case solution was 1.03% higher than that predicted by the two-dimensional solution used to design the shape.

Table 1 Wind-tunnel model designed for Mach 6.4

Drag, N	Sw, m^2	Volume, m^3	R_{eff}, m	C
6.39×10^1	5.26×10^{-2}	2.34×10^{-4}	3.34×10^{-2}	5.02×10^{-2}
7.67×10^1	5.50×10^{-2}	2.80×10^{-4}	3.66×10^{-2}	5.68×10^{-2}
9.18×10^1	5.77×10^{-2}	3.30×10^{-4}	3.97×10^{-2}	6.35×10^{-2}
1.30×10^2	6.39×10^{-2}	4.39×10^{-4}	4.58×10^{-2}	7.69×10^{-2}
1.80×10^2	6.95×10^{-2}	5.65×10^{-4}	5.20×10^{-2}	9.03×10^{-2}

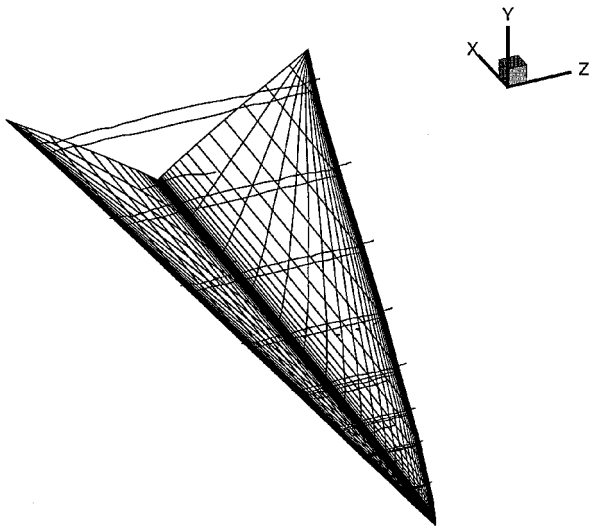

Fig. 7 Pressure contours from a three-dimensional calculation of a power law starbody at Mach 6.4.

Predicted Performance

To analyze the benefits of using a power law starbody design, the drag is calculated for different sized bodies. These calculations are then compared to those of planar starbodies and cones of equivalent volume and length. All calculations are made assuming zero base pressure on the rear of the body. The forces are calculated by integrating the pressures taken from the inviscid two-dimensional solution over the surface of the body and approximating the viscous drag using a reference temperature method.[9] Because of the larger surface area of the starbody designs, the performance benefits vary with the length of the model. Two cases are investigated to explore these differences. The performance of a wind-tunnel model, 0.2 m in length, is studied. A 1.5-m-long, large-scale body is also looked at to represent a more practical application, such as a hypersonic missile, where the benefits of using such a forebody are even more apparent. In each of these cases, the number of fins n is held fixed at 4. This is to ensure that the angle between the fin walls is large, such that any interaction of the boundary layers of the two walls would be minimized.

Performance of a Wind-Tunnel Model

In the design of a test model, the length of the body was held fixed, and the radius of the generating power law was allowed to vary. The freestream conditions for the computational solution were $P_\infty = 6345$ Pa, $T_\infty = 439$ K, $\rho_\infty = 0.05$ kg/m^3, and $M_\infty = 6.4$. The results for a range of generating radii are shown in Table 1.

The total drag on comparable wedge-derived starbodies, axisymmetric power law bodies, and cones was calculated to determine the performance benefits. The figure of merit chosen for comparison was the effective radius R_{eff}. This is the radius of a cone with the

Table 2 Large-scale model designed for Mach 6.4

Drag, N	Sw, m^2	Volume, m^3	R_{eff},, m	C
2.95×10^4	2.8412	8.36×10^{-2}	2.31×10^{-1}	0.223
4.17×10^4	3.0191	1.08×10^{-1}	2.62×10^{-1}	0.267
5.72×10^4	3.2250	1.35×10^{-1}	2.93×10^{-1}	0.312
7.69×10^4	3.4278	1.66×10^{-1}	3.25×10^{-1}	0.357
1.01×10^5	3.6344	1.99×10^{-1}	3.56×10^{-1}	0.401
1.49×10^5	3.9819	2.55×10^{-1}	4.03×10^{-1}	0.468

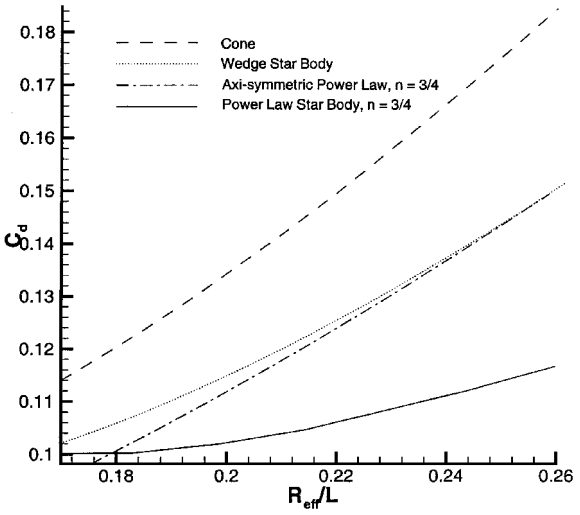

Fig. 8 Performance comparison of various bodies at Mach 6.4; wind-tunnel model.

same volume and length as the body. A drag coefficient was computed based on the total drag (viscous drag plus wave drag) and the cross-sectional area of an equivalent cone ($S = \pi R_{\text{eff}}^2$). The length of each body was held fixed at $L = 0.2$ m, and the number of fins was held fixed at $n = 4$. A direct comparison of the drag coefficients for each type of body is shown in Fig. 8. As can be seen, the power law starbody performs significantly better than the wedge starbody and the equivalent cone. The starbody also performs better than a comparable axisymmetric power law; however, this occurs only for shapes where the equivalent cone has a half-angle of greater than 9.5 deg. For smaller shapes, the larger viscous drag associated with the power law star becomes more significant, and the total drag exceeds that of its axisymmetric counterpart. However, the drag curves quickly diverge for larger shapes. The power law starbody drag curve slope remains fairly small, and a body with a much larger effective radius can be chosen for a given amount of drag.

Performance of a Large-Scale Model

The length of the large-scale model was fixed at 1.5 m, and the radius of the generating power law was allowed to vary, just as in the wind-tunnel model case. The freestream conditions for the computational solution were chosen as standard atmosphere conditions at sea level: $P_\infty = 101$ MPa, $T_\infty = 300$ K, $\rho_\infty = 1.17$ kg/m^3, and $M_\infty = 6.4$. The results for a range of generating radii are shown in Table 2.

The calculations were similar to those of the wind-tunnel model case, except that the length was fixed at $L = 1.5$ m. R_{eff} and C_d were calculated based on a cone of equivalent volume and length. A comparison of the drag coefficients for the power law starbody and comparable wedge-derived starbodies, axisymmetric power law bodies, and cones is shown in Fig. 9. The results are similar to those presented in Fig. 8. The main difference is that the viscous drag for the larger model is a smaller percentage of the total drag. As such, the performance difference between the power law starbody and an equivalent cone is even larger than in the wind-tunnel model case. It is also important to note that the power law star performs better than the axisymmetric power law, due to the reduced impact of the viscous drag for the 1.5-m case.

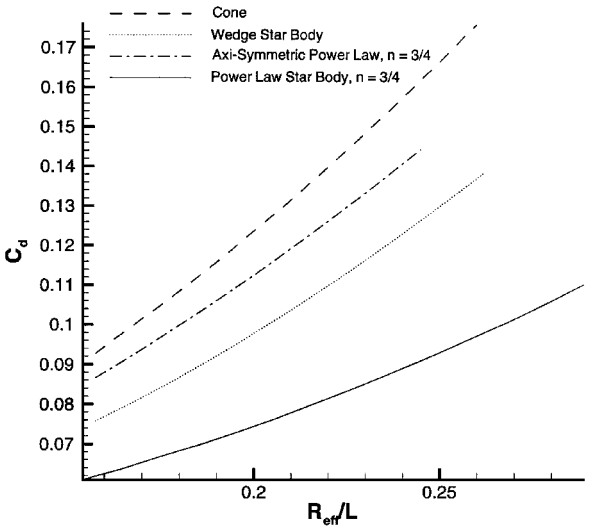

Fig. 9 Performance comparison of various bodies at Mach 6.4; large-scale model.

Experimental Setup and Results

Starbody Model

The starbody model for the test was designed using a $\frac{3}{4}$-power law centerline 200 mm long and 18 mm in height, with the freestream Mach number set at 6.4 and the freestream $\gamma = 1.4$. The resulting starbody design had a volume of 3.054×10^{-4} m^3 and an effective radius $R_{\text{eff}} = 38.2$ mm. This design is equivalent in volume to a cone 200 mm long with a half-angle of $\theta = 10.8$ deg. The number of fins n was chosen as 4 to limit the amount of skin-friction drag and to minimize the boundary-layer interaction between two adjacent fins at the centerline.

To remove the base pressure on the model, a hollow buffer was constructed and was placed 1–2 mm from the base of the model. Because the test section is evacuated, the pressure inside this buffer is negligible. At the interface between the buffer and the model, some flow will enter the buffer. At this interface, the flow is assumed to choke. The pressure at this interface is assumed to be acting on the base of the model over a length equal to the thickness of the buffer, 3 mm. The original drag predictions that assumed zero base pressure are then corrected using this value.

Force Measurement

The technique used for measuring the drag force on a model in a short-duration shock-tunnel flow is referred to as the *stress wave force-balance technique*. It was developed at the University of Queensland through the initial work of Sanderson and Simmons[10] and Tuttle et al.[11] A brief description of the technique is given here, but full details of the operation of the stress wave force balance can be found in Refs. 10 and 11. The technique has subsequently been applied to measurements such as the thrust developed by a fueled scramjet-powered vehicle[12] and has been extended to measurement of three components of force.[13]

The drag balance comprises the aerodynamic model attached to a long, hollow stress bar. The bar is supported horizontally in the test section by fine wires, which are arranged to allow the model to move freely in the direction of the drag force. The stress bar and support wires are shielded from the flow so that only the model experiences an aerodynamic drag force. Strain gauges are bonded to the stress bar downstream of its attachment to the model. When the flow arrives (impulsively) in the test section, the sudden application of a drag force on the model sets up stress waves, which propagate and reflect within the model. This stress wave activity is transmitted to the stress bar and is sensed by the strain gauges. Changes in the aerodynamic force on the model lead to further stress wave initiation and propagation. The arrangement is modeled as a linear system in which the measured strain time history $y(t)$ can be related to the

drag force on the model $u(t)$ via an impulse response function $g(t)$ using a convolution integral:

$$y(t) = \int_0^t g(t-\tau)u(\tau)\,\mathrm{d}\tau \tag{1}$$

The time history of the drag force on the model can then be found using deconvolution techniques. In the present experiments, the deconvolution routines are based on the extended-conjugate-gradient time-domain algorithm of Prost and Goutte.[14] The accuracy with which drag forces can be measured with this technique and the present instrumentation is ±10% (Ref. 11).

Table 3 Test conditions in T4

Enthalpy, MJ/kg	Mach number	Pressure, kPa	Temperature, K	Velocity, m/s
3.3	6.55	6.49	341	2422
4.0	6.35	6.35	439	2664
5.6	6.26	7.64	610	3072
10.8	5.55	9.67	1397	4083
5.57 ($Re = 2.0 \times 10^6$)	6.18	10.84	627	3072
4.76 ($Re = 0.5 \times 10^6$)	6.54	2.42	455	2792

Table 4 Percent difference in measured drag coefficient between the starbody and the cone

Enthalpy, MJ/kg	Drag difference, %
3.3	19.3
4.0	20.5
5.6	17.4
10.8	4.0

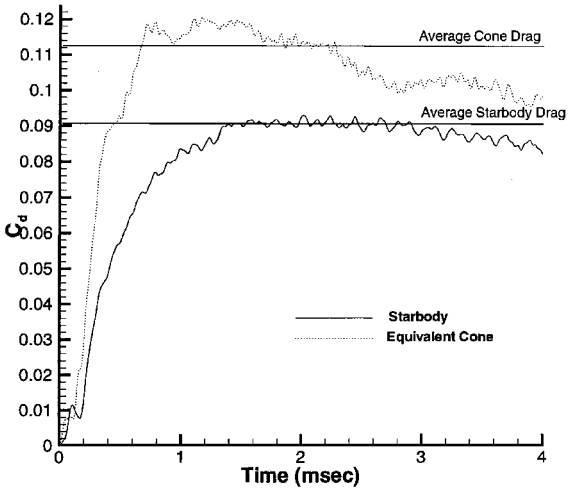

Fig. 10 Drag comparison at 3.3-MJ/kg test condition.

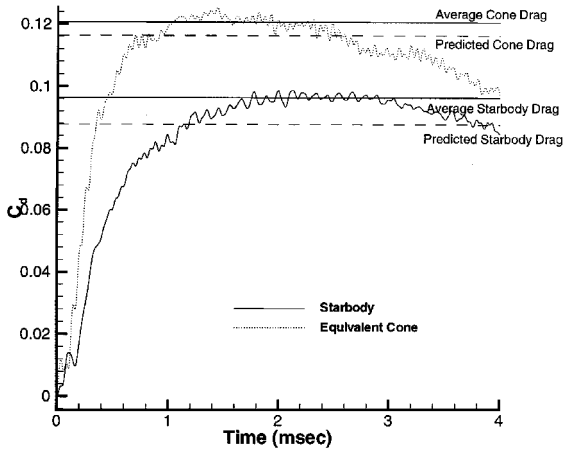

Fig. 11 Drag comparison at 4.0-MJ/kg test condition.

Test Conditions

Various enthalpies were used to vary the test section Mach number. The design point enthalpy, 4.0 MJ/kg, and three other enthalpies were chosen. For the purpose of investigating scaling effects, two

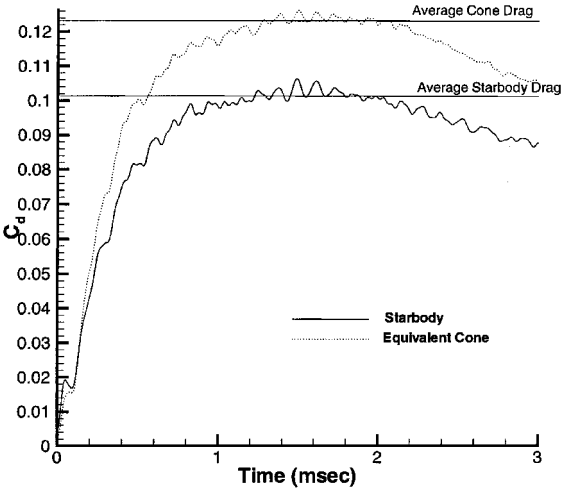

Fig. 12 Drag comparison at 5.6-MJ/kg test condition.

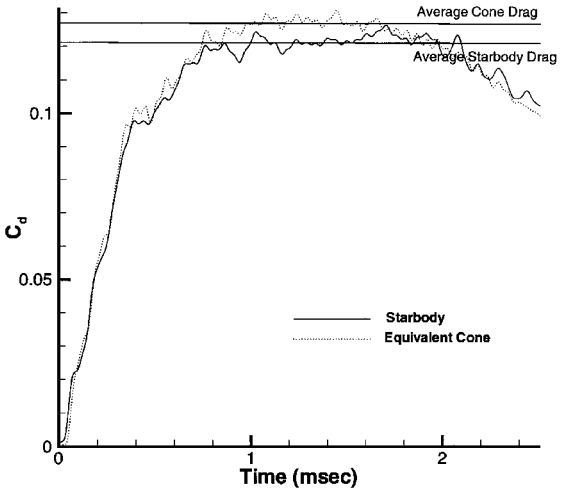

Fig. 13 Drag comparison at 10.8-MJ/kg test condition.

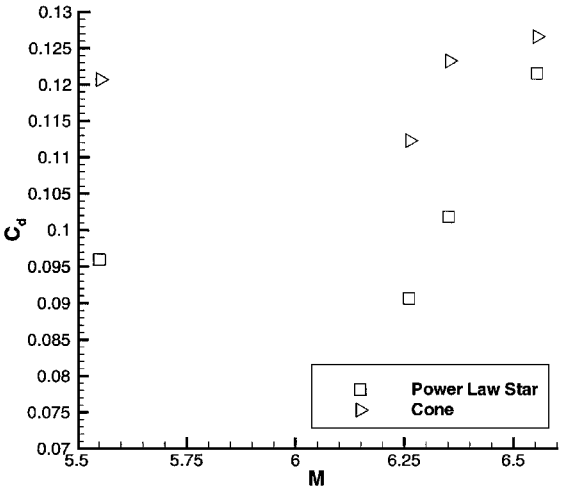

Fig. 14 Drag comparison for baseline test conditions.

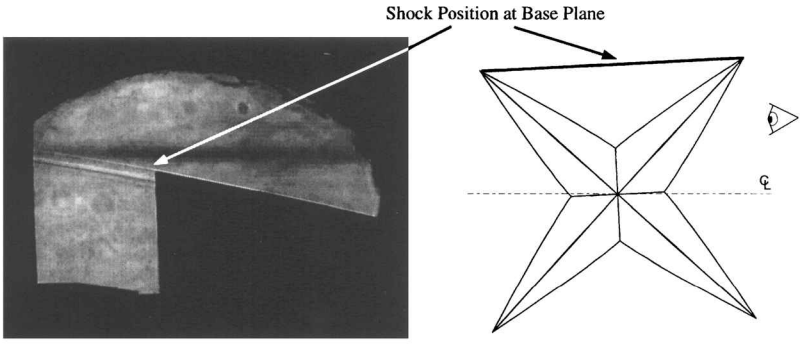

a) Side view of trailing-edge shock b) Cross-sectional view at base plane

Fig. 15 Shadowgraph of starbody at 4.0-MJ/kg test condition.

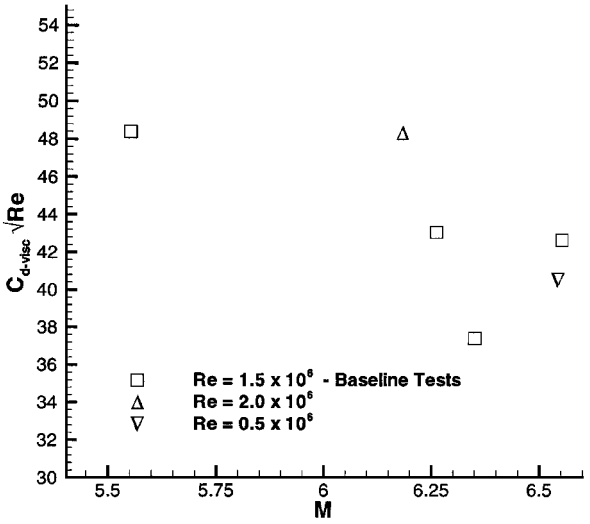

Fig. 16 Viscous drag normalized by Reynolds number.

additional tests were conducted at higher and lower Reynolds numbers. The resulting test section conditions are shown in Table 3.

Results

The resulting drag acting on both the starbody and the equivalent cone for each of the baseline test conditions is shown in Figs. 10–13. The drag is averaged over the test time to determine a drag value against which to compare the predictions. These values, for each of the baseline test conditions, are shown in Fig. 14. For the 4.0-MJ/kg test case, the on-design test case, the predicted drag difference between the starbody and the cone was 24.9%, whereas the measured difference was 20.5%. The measured differences in drag for all of the test cases are shown in Table 4.

As can be seen, at the on-design condition, the starbody provides a substantial drag savings, even at the Reynolds numbers of 1.5×10^6 in this experiment. The starbody continues to perform well at Mach numbers close to the on-design condition; however, the performance benefits diminish at off-design conditions, as can be seen in the 10.8-MJ/kg case.

To further verify that the predicted flowfield was being produced, shadowgraphs were produced to ensure that the shock was attached to the fins of the model (Fig. 15a). The photograph shows the base region of the starbody, without the buffer. The two-dimensional shock wave does not appear along the edge of the fins in the photograph; however, it can be seen that the shock wave leaves the model at the tips of the fins, clearly showing that this shock wave is attached to fins. Two shock waves seem to appear in the shadowgraph; however, this is due to the model being slightly rotated by approximately 3 deg on the sting. These waves are actually a single shock wave that is at an angle to the observer. This orientation, with respect to the observer, is shown in Fig. 15b.

Two additional tests were conducted to investigate the effect of scaling on the performance of the starbody. Because of the difficulty in producing test conditions comparable to those of the baseline case, an additional analysis was performed on these results. A change in Reynolds number should result in a change in viscous drag, but the pressure drag should remain constant. An analysis using three-dimensional CFD results was done, with an approximation of the viscous drag, for each of the baseline cases. In each case, the viscous drag was between 32 and 34% of the total drag calculated. Using this value, the measured drag coefficients C_d for each of the baseline cases were divided into a drag coefficient due to pressure drag $C_{d\text{-press}}$ and a drag coefficient due to viscous drag $C_{d\text{-visc}}$. For the higher- and lower-Reynolds-number cases, the value of $C_{d\text{-press}}$ was interpolated from the baseline case results to approximate the pressure drag acting on the starbody, based on the Mach number. The value of $C_{d\text{-visc}}$ can then be determined by subtracting this approximate $C_{d\text{-press}}$ from the measured C_d. Each value of $C_{d\text{-visc}}$ is then normalized by multiplying by $\sqrt{Re}$. The resulting plot for all of the test cases is shown in Fig. 16. The difference between the off-design Reynolds number tests and the baseline is approximately $\pm 10\%$. This difference is just within the tolerance of the force balance. Other errors may have been introduced in the approximation of the pressure drag. Boundary-layer transition in the tunnel occurs for Reynolds numbers between 1.0×10^6 and 1.5×10^6 and may have occurred on the model, introducing another source of error in the viscous drag predictions.

Conclusions

The major benefit of using a power law starbody is to decrease the drag per volume for a forebody of fixed length. Depending on the application, such a body has the potential for increasing the effective payload size of a given vehicle or projectile. As was shown through both computations and experiment, such a configuration can have 20% less drag than a 10.8-deg equivalent cone. For large-scale applications, the performance benefits should increase.

The agreement of the measured values to the predicted values is good. The drag difference between measured and predicted values for the starbody was 9.5% and was within the uncertainty of the force balance. The error in the prediction for the starbody and for the cone appeared to be systematic, suggesting that the viscous forces are underpredicted using the reference temperature method. It was shown that the flowfield was behaving as intended, as the shock wave was attached to the fins.

The off-design Reynolds number tests are promising. These results seem to confirm a simple dependence on $1/\sqrt{Re}$, suggesting that the starbody would perform even better for larger-scale applications. This analysis assumed laminar flow, which holds for most of the experiments conducted; however, a calculation of the turbulent viscous drag contribution would be necessary for a more accurate estimation of the performance for larger-scale applications.

Acknowledgments

This work was supported, in part, by NASA Grant NGT 52158, with Charles Cockrell Jr. as Technical Monitor, to whom appreciation is expressed. This work was also supported by the Center of Hypersonics Education and Research, NASA NAGw 11796, with Isaiah Blankson at the NASA Lewis Research Center as Technical Monitor, to whom appreciation is expressed. Appreciation is also expressed to Michael Smart for his technical input. Gratitude is expressed to James Randolph at the Supercomputing Center at the Jet Propulsion Laboratory for the generous allocation of Cray CPU time. Appreciation is expressed to Anthony Gardner for his work in producing the shadowgraphs for this experiment.

References

[1]Chernyi, G. G., and Gonor, A. L., "Transversal Contour of Minimum Pressure Drag," *Theory of Optimum Aerodynamic Shapes*, edited by A. Miele, Academic, New York, 1965, pp. 283–295.

[2]Vedernikov, Y., Gonor, A., Zubin, M., and Ostapenko, N., "Aerodynamic Characteristics of Star-Shaped Bodies at Mach Numbers $M = 3$–5," *Izvestiya Akademii Nauk SSSR, Mekhanika Zhidkosti i Gaza*, No. 4, July–Aug. 1981, pp. 88–93.

[3]Zubin, M. A., Lapygin, V., and Ostapenko, N., "Theoretical and Experimental Investigation into the Structure of Supersonic Flow Past Bodies of Star-Shaped Form and Their Aerodynamic Characteristics," *Izvestiya Akademii Nauk SSSR, Mekhanika Zhidkosti i Gaza*, No. 3, May–June 1982, pp. 34–40.

[4]Foster, N., and Dulikravich, G., "Aerodynamic Characteristics of Star-Shaped Bodies at Mach Numbers $M = 3$–5," *Journal of Spacecraft and Rockets*, Vol. 34, No. 1, 1997, pp. 36–42.

[5]Sabean, J., and Lewis, M., "A Parametric Study of Star Bodies for Minimum Drag," *Proceedings of the 21st International Symposium on Shock Waves*, Paper 7998, 1997.

[6]*GASP Version 3.0*, Aerosoft, Inc., Blacksburg, VA, May 1996.

[7]O'Neill, M., and Lewis, M., "Optimized Scramjet Integration on a Waverider," *Journal of Aircraft*, Vol. 29, No. 6, 1992, pp. 1114–1121.

[8]Rasmussen, M., *Hypersonic Flow*, Wiley, New York, 1994, pp. 101–128.

[9]Eckert, E., "Laminar and Turbulent Boundary-Layer Flow over Surfaces with Constant Pressure and Temperature," *Transactions of the American Society of Mechanical Engineers*, Vol. 78, Aug. 1956, p. 590.

[10]Sanderson, S., and Simmons, J., "Drag Balances for Hypervelocity Impulse Facilities," *AIAA Journal*, Vol. 29, No. 12, 1991, pp. 2185–2191.

[11]Tuttle, S., Mee, D., and Simmons, J., "Drag Measurements at Mach 5 Using a Stress Wave Force Balance," *Experiments in Fluids*, Vol. 19, No. 5, 1995, pp. 336–341.

[12]Paull, A., Stalker, R., and Mee, D., "Experiments on Supersonic Combustion Ramjet Propulsion in a Shock Tunnel," *Journal of Fluid Mechanics*, Vol. 296, 1995, pp. 159–183.

[13]Mee, D., Daniel, W., and Simmons, J., "Three-Component Force Balance for Flows of Millisecond Duration," *AIAA Journal*, Vol. 34, No. 3, 1996, pp. 590–595.

[14]Prost, R., and Goutte, R., "Three-Component Force Balance for Flows of Millisecond Duration," *Signal Processing*, Vol. 7, No. 3, 1984, pp. 209–230.

R. M. Cummings
Associate Editor